Determining and Visualizing Uncertainty in Estimates of Fiber Orientation From Diffusion Tensor MRI

Derek K. Jones*

Diffusion tensor MRI (DT-MRI) permits determination of the dominant orientation of structured tissue within an image voxel. This has led to the development of 2D graphical methods for representing fiber orientation and DT-MRI "tractography," which aims to reconstruct the 3D trajectories of white matter fasciculi. Most contemporary fiber orientation mapping schemes and tractography algorithms employ the directional information contained in the eigenvectors of the diffusion tensor to approximate white matter fiber orientation. However, while the uncertainty associated with every estimate of an eigenvector has long been recognized, no attempts to quantify this uncertainty in vivo have been reported. Here, a method is proposed for determining confidence intervals in fiber orientation from real DT-MRI data using the bootstrap method. This is used to construct maps of the "cone of uncertainty," allowing simultaneous viewing of fiber orientation and its uncertainty, and to examine the relationship between orientation uncertainty and tissue anisotropy. Magn Reson Med 49:7–12, 2003.

Key words: diffusion tensor; eigenvector; uncertainty; tractography

That diffusion is anisotropic in white matter has been known for over a decade (1). The observation that the apparent diffusivity of water is greatest along the dominant orientation of white matter tracts within an image voxel has led to a variety of methods for displaying fiber orientation, ranging from simple techniques based on apparent diffusion coefficients measured in two orthogonal directions (2), to methods based on information contained within the full diffusion tensor (3–6). This orientational information has been further exploited in attempts to infer axonal connectivity in the brain (7–13). In the majority of these methods, at each step in the reconstruction of a fiber trajectory a single estimate of fiber orientation is used to determine the direction of propagation.

There are two factors that are important for reliable fiber orientation mapping and tractography: 1) accuracy of the estimates of fiber orientation, and 2) repeatability/precision of the estimates. In this work, we shall only consider the latter. Due to the noise inherent in all MR images, there is an uncertainty associated with every estimate of fiber orientation. In tractography, accumulated uncertainties in fiber orientation have clear potential for leading to erroneous reconstructions of pathways. Some approaches have attempted to allow for the uncertainty in fiber orientation (9,13), or have attempted to reduce the uncertainty in fiber orientation either through regularization approaches (10,14) or through generating continuous approximations to the sampled tensor field and applying smoothing factors (15,16).

Similarly, in fiber orientation display methods, a single fiber orientation is depicted for each image voxel, with no indication of the uncertainty in fiber orientation. This problem, of course, is not unique to display of eigenvector data from DT-MRI, but is common to all displays of vectorial data — such as those obtained from meteorological stations or from Doppler radars. The interpretation of vectorial data would be more effective if this uncertainty could be displayed together with the original data. Wittenbrink et al. (17) discussed this issue in some depth and described various glyphs for visualizing uncertainty in vector fields. Basser (18) later described an approach for constructing such a glyph or a "cone of uncertainty" in the estimate of eigenvectors obtained from DT-MRI, i.e., a cone whose cone angle is equal to the uncertainty (i.e., a given confidence interval) in the estimate of the orientation of the principal eigenvector. However, this method was based on matrix perturbation analysis of synthetic data. No attempts to determine the uncertainty of estimates of fiber orientation in vivo from real data have yet been reported.

The bootstrap method (19) is a nonparametric procedure that enables one to estimate the uncertainty of a given statistic, or its probability density function (PDF). It does so by randomly selecting individual measurements (in this case individual diffusion-weighted images), with replacement, from a set of repeated measurements, thus generating many bootstrap samples. Each bootstrap sample provides a random estimate of a given statistic. Hence, by generating a sufficient number of the bootstrap replicates one obtains a measure of uncertainty or, in some cases, the PDF of the given statistic. For the purposes of explanation, suppose that we have a pool of data from which we draw n samples and input them into a model to compute a parameter of interest, θ. An approximate sampling distribution for θ can be obtained by repeating the following procedure N_b times, (where N_b stands for "number of bootstraps"):

1) From the pool of data, draw a sample of n input parameters for input to the model, with replacement. We shall refer to this sample as the j^{th} "bootstrap sample."
2) Compute the parameter of interest from the bootstrap sample, which we refer to as the j^{th} bootstrap estimate θ^j.

The collection of N_b bootstrap estimates (θ^j, $j = 1 \ldots N_b$) all represent possible estimates of θ based on configurations of the observed data, and can therefore be used to

Section of Old Age Psychiatry, Institute of Psychiatry, De Crespigny Park, London, UK, and Division of Medical Physics, Leicester Royal Infirmary, Infirmary Square, Leicester, UK.

Grant sponsor: Wellcome Trust; Grant number: 054030/JHW/JP/JAT.

*Correspondence to: Derek K. Jones, NIH, Rm. 3W16E, Bldg. 13, 13 South Drive, Bethesda, MD. E-mail: jonesde@mail.nih.gov

Received 10 April 2002; revised 8 August 2002; accepted 9 September 2002.
DOI 10.1002/mrm.10331
Published online in Wiley InterScience (www.interscience.wiley.com).

approximate the form of the true distribution of the parameter estimate. It is therefore possible, from the distribution, to determine confidence intervals for the parameter of interest, θ.

Recently, Pajevic and Basser (20) proposed a nonparametric method for statistical analysis of DT-MRI data based on the bootstrap method. In this implementation of the bootstrap, a set of n diffusion-weighted images is collected as part of a DT-MRI imaging experiment. From this pool of n images, a subset of N_{DWI} images, (where $N_{DWI} < n$), is drawn and used to compute the diffusion tensor in each voxel. If the acquisition of the N_{DWI} images is repeated N_R times (i.e., $n = N_{DWI} \times N_R$), then there are $(N_R)^{N_{DWI}}$ possible configurations of the N_{DWI} images that can be used to compute estimates of the diffusion tensor within each voxel, i.e., for each of the N_{DWI} images used to compute the diffusion tensor there are N_R to choose from. Pajevic and Basser (20) used this approach to derive distributions of the elements of the diffusion tensor, its eigenvalues, its trace, and measures of anisotropy. This application of the bootstrap procedure has also been used by other groups to compare the performance of DT-MRI acquisition schemes (21) and tractography algorithms (22) and is clearly a useful tool in terms of characterization of noise in DT-MRI data.

Here we present a method to determine the cone of uncertainty directly from diffusion imaging data in vivo using the bootstrap method. We show how to determine confidence intervals in fiber orientation and how to represent this in an iconic map of the cone of uncertainty, allowing both fiber orientation and uncertainty to be visualized concurrently.

MATERIALS AND METHODS

Data Acquisition

Two complete volumes of DT-MRI data were acquired from a healthy volunteer on a GE Signa LX system (General Electric, Milwaukee, WI), with actively shielded magnetic field gradients (maximum amplitude 40 mT m^{-1}). A standard quadrature birdcage head coil was used for both RF transmission and NMR signal reception.

Each volume was acquired using a multislice peripherally gated EPI sequence, optimized for precise measurement of the diffusion tensor in parenchyma, from a healthy volunteer, from 60 contiguous near-axial slice locations with isotropic (2.5 × 2.5 × 2.5 mm) resolution. The echo time was 107 ms while the effective repetition time was 15 R-R intervals. The duration of the diffusion encoding gradients was 17.3 ms, giving a maximum diffusion weighting of 1300 s mm^{-2}. At each slice location, seven images were acquired with no diffusion gradients applied, together with 64 diffusion-weighted images in which gradient directions were uniformly distributed in space. Full details are given elsewhere (23).

A vacuum device and surgical tape were used to minimize head motion. Subtraction of corresponding images from the two datasets verified that motion between the two scans was negligible. The subject's consent was obtained, according to the declaration of Helsinki, and the scanning protocol was approved by the local Ethical Committee.

Analysis

To generate the j^{th} bootstrap sample for a particular slice, one of the two images acquired with each b-matrix was randomly selected (with replacement) to produce a dataset consisting of 71 diffusion-weighted images. Log-linear regression was used to estimate the tensor in each voxel (24) and the principal eigenvector, $\boldsymbol{\varepsilon}_1$, was determined. This procedure was repeated 1000 times to generate 1000 bootstrap estimates of $\boldsymbol{\varepsilon}_1$.

Following Basser and Pajevic (25), in each voxel we then calculated the mean dyadic tensor, $\langle \varepsilon_1^j \varepsilon_1^{jT} \rangle$, for the 1000 bootstrap estimates, where:

$$\langle \varepsilon_1^j \varepsilon_1^{jT} \rangle = \left\langle \begin{pmatrix} (\varepsilon_{1x}^j)^2 & \varepsilon_{1x}^j \varepsilon_{1y}^j & \varepsilon_{1x}^j \varepsilon_{1z}^j \\ \varepsilon_{1x}^j \varepsilon_{1y}^j & (\varepsilon_{1y}^j)^2 & \varepsilon_{1y}^j \varepsilon_{1z}^j \\ \varepsilon_{1x}^j \varepsilon_{1z}^j & \varepsilon_{1y}^j \varepsilon_{1z}^j & (\varepsilon_{1z}^j)^2 \end{pmatrix} \right\rangle = \frac{1}{1000} \sum_{j=1}^{1000} \varepsilon_1^j \varepsilon_1^{jT}, \quad [1]$$

and ε_{1i}^j is the i^{th} component of the j^{th} bootstrap estimate of the principal eigenvector.

Note that for each individual dyadic tensor, there is only one nonzero eigenvalue. The eigenvector of the dyad that is associated with this eigenvalue is parallel to the eigenvector from which the dyad is formed. Thus, the dyadic formalism provides a convenient method for averaging eigenvectors which handles the problem of antipodal symmetry, i.e., the eigenvector is only defined up to its orientation along a particular axis. The principal eigenvector, $\bar{\Psi}_1$ of the average dyad, $\langle \varepsilon_1^j \varepsilon_1^{jT} \rangle$, was then determined, together with its three eigenvalues, assigned here as β_1, β_2, and β_3.

The coherence, κ, of the 1000 estimates, $\varepsilon^j{}_1$, was subsequently characterized in each voxel using :

$$\kappa = \left(1 - \sqrt{\frac{\beta_2 + \beta_3}{2\beta_1}} \right) \quad [2]$$

which is formed from the dispersion measure proposed by Basser and Pajevic (25). This measure takes values from zero (when all the $\varepsilon^j{}_1$ are uniformly distributed over the unit-sphere, and $\beta_1 = \beta_2 = \beta_3$) to unity (when all the $\varepsilon^j{}_1$ are collinear and $\beta_2 = \beta_3 = 0$).

Next, for each voxel the minimum angle subtended between each bootstrap estimate, $\boldsymbol{\varepsilon}_1{}^i$, and the average principal eigenvector, $\bar{\Psi}_1$, was determined from

$$\theta^j = \text{acos}(\varepsilon_1^j \cdot \bar{\Psi}_1) \quad [3]$$

There are four main approaches to computing bootstrap confidence intervals — normal approximation, percentile, bias-corrected percentile, and percentile-t (26). As the bootstrap procedure produces a large sample from the sampling distribution of a statistic, the most straightforward approach for determining confidence intervals is taking quantiles. It has been shown that this method generates intervals with correct asymptotic coverage (26). To compute confidence intervals for the estimates of fiber orientation, we therefore employed the percentile method. The usual procedure is to order the set of bootstrap estimates, θ, and determine the lower bound for the (1-α) × 100 confidence interval as the $((\alpha/2) \times N_b)$th value and the

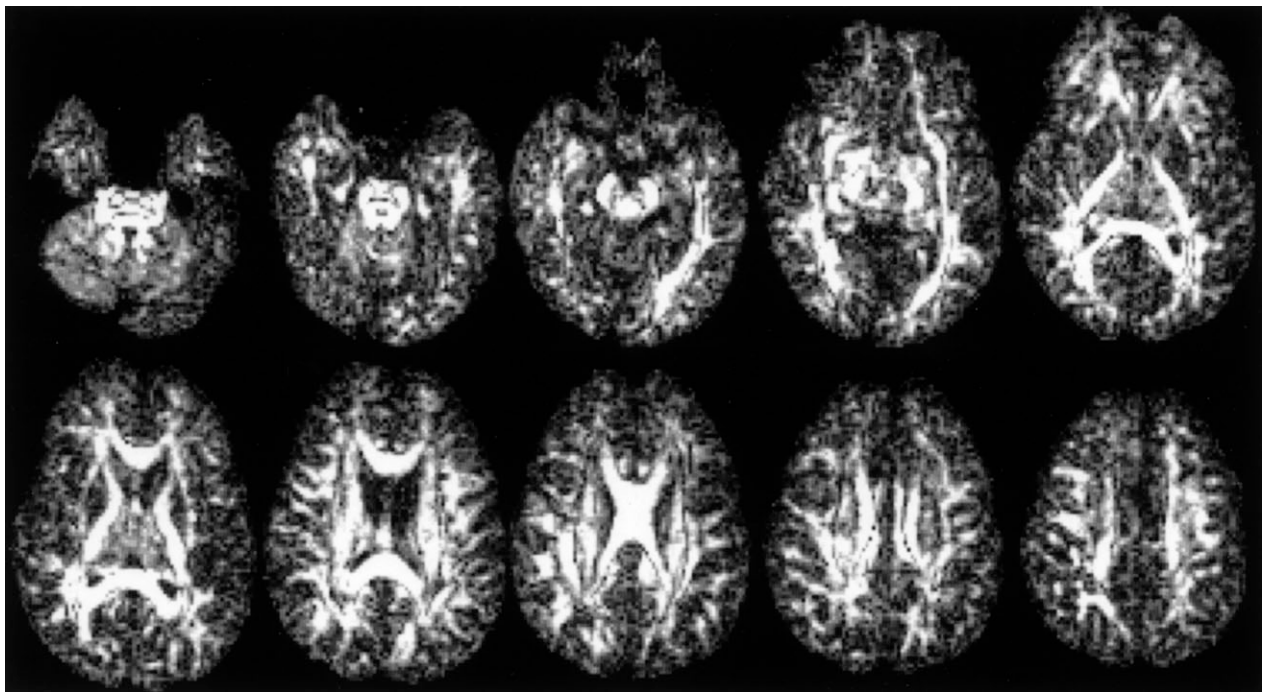

FIG. 1. Coherence, κ, of 1000 bootstrap estimates of the principal eigenvector, $\varepsilon_{1,}$ in each voxel for 10 different slice locations.

upper bound as the ((1-(α/2)) $\times$ N_b)th value. However, since in this case the values of θ^j are computed from Eq. [3] and are therefore always greater than zero, the distribution is by definition "one-tailed." Hence, the value of θ at the 950th position in the list of 1000 represents the 95% confidence interval. In each voxel, by constructing a cone with a cone angle corresponding to this confidence interval, with a long axis coincident with the mean eigenvector, $\bar{\Psi}_1$, a glyph was created which allowed both fiber orientation and uncertainty to be visualized concurrently.

To examine the relationship between uncertainty in fiber orientation and anisotropy, we created a scatterplot of the 95% confidence interval in fiber orientation vs. anisotropy, plotting the data for every voxel in the entire 60-slice volume. The measure used to quantify anisotropy was "C_{linear}," proposed by Westin et al. (27). This measure is a component of the barycentric coordinate system that describes the geometry of the diffusion tensor in terms of its "cigar-like" (C_{linear}), "disk-like" shape (C_{planar}), and "spherical" ($C_{spherical}$) coordinates.

C_{linear} is defined as:

$$C_{linear} = \frac{\lambda_1 - \lambda_3}{\lambda_1 + \lambda_2 + \lambda_3}, \qquad [4]$$

where λ_1, λ_2, and λ_3, are the rank-sorted eigenvalues of the diffusion tensor.

RESULTS

Figure 1 shows the orientational coherence, κ, of the 1000 bootstrap estimates of ε_1 formed according to Eq. [2], for a range of slice locations in the brain. The image intensity is directly proportional to κ. Note that in central anisotropic structures the coherence is large, i.e., the uncertainty in the principal eigenvector estimates is small. 95% confidence interval are given in Table 1 for the splenium, body, and genu of corpus callosum, the cerebral peduncles, the internal capsule, and the frontal white matter.

Figure 2 shows cones of uncertainty (at the 95% confidence level) in a region at the level of the splenium of the corpus callosum. Note that where the underlying fibers merge or cross and the voxel-averaged anisotropy becomes low (the zoomed region), the uncertainty in ε_1 becomes large.

Figure 3 shows the 95% confidence interval in fiber orientation vs. C_{linear}. Note that even at high anisotropy, the smallest 95% confidence interval in fiber orientation is approximately 2.5° and at values of C_{linear} lower than approximately 0.15 the uncertainty in fiber orientation rises sharply.

DISCUSSION

We have shown how to determine uncertainty in estimates of fiber orientation obtained by DT-MRI, how to determine

Table 1
95% Confidence Intervals in Fiber Orientation Estimates in Different White Matter Regions

Brain region	95% Confidence interval
Splenium	± 2.9°
Body of corpus callosum	± 3.5°
Genu of corpus callosum	± 4.8°
Cerebral peduncles	± 3.2°
Internal capsule	± 8.2°
Frontal white matter	± 10°

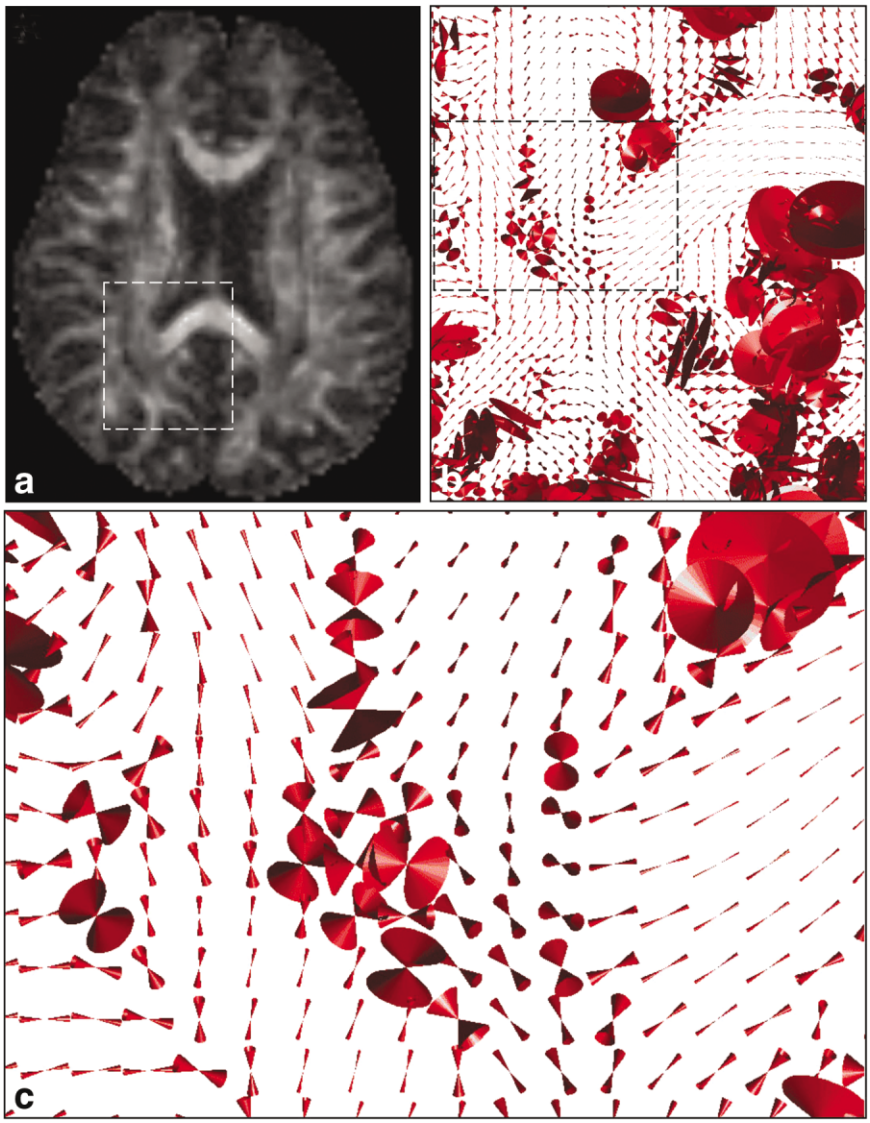

FIG. 2. Cones of uncertainty (showing the 95% confidence angle) at the level of the splenium of the corpus callosum. **a:** Fractional anisotropy. **b:** Cones of uncertainty in the region indicated by the dashed lines in **a**. This region is further magnified in **c**. The zoomed area highlights a region where fibers cross and the uncertainty in ε_1 is large.

confidence intervals, and how to visualize both fiber orientation and uncertainty concurrently. Since this technique provides an objective measure of reproducibility of fiber orientation, it could be used to provide objective comparison of the performance of different DT-MRI data acquisition strategies in terms of their reproducibility of fiber orientation.

This technique could also be used to compare the efficacy of different tensor smoothing and regularization techniques (10,14–16) which aim to eliminate variations in estimates of eigenvectors due to noise while preserving true anatomical variations. The optimal scheme would be that which resulted in the smallest cone of uncertainty while, at the same time, introducing minimum perturbation of the most probable fiber orientation (i.e., the most likely fiber orientation in the unsmoothed/unregularized data).

Both Figs. 1 and 2 show low uncertainty in fiber orientation estimates in the splenium of the corpus callosum, a structure that is much favored in the tractography literature. It is perhaps unsurprising, therefore, that results ap-

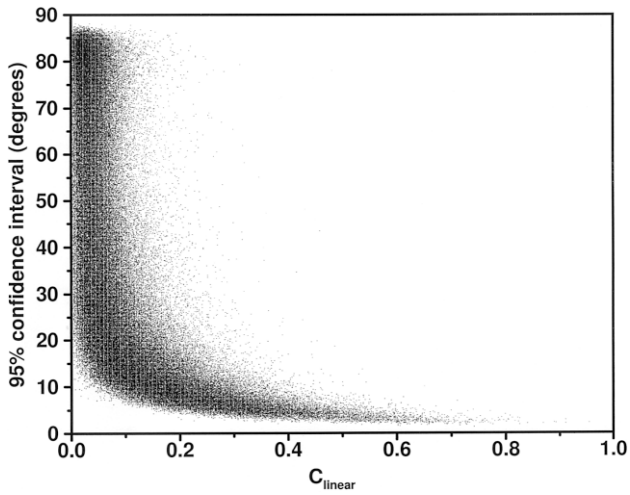

FIG. 3. Plot of 95% confidence interval in fiber orientation vs. C_{linear}. The data for each voxel in the entire 60-slice volume are plotted on a pair-wise basis.

pear to be consistent across different tractography algorithms in this region. However, in the regions where fibers cross or merge and the anisotropy becomes low (the zoomed region in Fig. 2), the uncertainty in fiber orientation is seen to be high. Tractography results obtained for tracts that pass through such regions are likely to be very irreproducible and it would therefore be interesting to perform repeatability studies of tract reconstructions both with the same algorithm and between different algorithms for tracts in these regions, again using the bootstrap method as first reported by Lazar et al. (22).

The plot presented in Fig. 3 shows, for the first time, the relationship between uncertainty in fiber orientation and anisotropy obtained in vivo. Plots such as this could be used to provide a more informed choice of anisotropy threshold for the termination of tracking in DT-MRI tractography algorithms. Such thresholds are usually selected arbitrarily on an ad hoc basis, assuming that tissue with anisotropy lower than the threshold will have an unacceptable uncertainty in fiber orientation.

We note that although the sorting of the eigenvalues necessary to compute C_{linear} (Eq. [4]) introduces bias in the presence of noise (28), we chose it over more commonly used measures such as fractional anisotropy and relative anisotropy (29) since these latter measures make no distinction between prolate and oblate tensors. In principle, when using these latter measures a prolate tensor and an oblate tensor can have the same anisotropy. In the oblate tensor, however, even if the anisotropy was high, the fiber orientation is poorly defined, which would result in a large 95% confidence interval.

In principle, the information about uncertainties in fiber orientation obtained by the method presented here could be incorporated into tractography algorithms to make probabilistic tract maps. Parker et al. (13) recently suggested a tractography algorithm that incorporated uncertainty in fiber orientation in order to make probabilistic connectivity maps. However, this assumed an ad hoc sigmoidal-shaped relationship between uncertainty in fiber orientation and anisotropy. The relationship between uncertainty in fiber orientation and anisotropy obtained here (Fig. 3) is somewhat different from that proposed by Parker et al. (13). Use of experimentally determined uncertainties, such as presented here, in combination with methods such as that suggested by Parker et al. (13) and also Koch et al. (11) should make such probabilistic maps obtained from DT-MRI more meaningful.

Xu et al. (30) have recently suggested a method for coregistering DT-MRI datasets in which knowledge of the probability density function (PDF) of the principal eigenvector within each voxel is required. In the absence of this knowledge, the authors employed a neighborhood sampling strategy in which the orientations of principal eigenvectors in a specific volume surrounding the voxel are used to construct an approximation to the PDF. Use of the strategy described in the present work provides a preferable way to determine the PDF for a particular voxel, as it constructs it directly using only data contained within the voxel itself.

We would like to stress that the results presented here are specific to our particular acquisition scheme. However, the *method* described here is quite general and is not specific to any particular acquisition scheme or model-based analysis. Given sufficient time, and cooperation of the volunteer, this approach could, in principle, be used to determine the reproducibility of orientational information obtained from alternative (higher-order) modeling approaches (31) — or model-free approaches (32).

Finally, we would like to stress that we have described a method for determining the *precision* of DT-MRI estimates of fiber orientation in vivo. It is important to note that this technique does not provide assessment of the *accuracy* of the estimates, for which comparison with a gold-standard is essential.

ACKNOWLEDGMENTS

This work was carried out during a visit to the Section on Tissue Biophysics & Biomimetics (STBB), Laboratory of Integrative & Medical Biophysics (LIMB), National Institute of Child Health & Human Development (NICHD). The author thanks Dr. Carlo Pierpaoli (NICHD) for assistance in the acquisition of data and Dr. Sinisa Pajevic (MSCL, CIT) for discussions relating to the bootstrap and for comments on the manuscript. I thank Dr. Mark Horsfield (University of Leicester) and Dr. Robert Howard and Dr. Fernando Zelaya (Institute of Psychiatry) for reading of the manuscript and helpful comments. Finally, I thank Dr. Larry Latour, Suburban Hospital, Bethesda, MD, for allowing access to the MR scanner where the data for this study were collected.

REFERENCES

1. Moseley ME, Cohen Y, Kucharczyk J, Mintorovitch J, Agari HS, Wendland HF, Tsuruda J, Norman D. Diffusion-weighted MR imaging of anisotropic water diffusion in cat central nervous system. Radiology 1990;176:439–445.
2. Douek P, Turner R, Pekar J, Patronas N, Le Bihan D. MR color mapping of myelin fiber orientation. J Comput Assist Tomogr 1991;15:923–929.
3. Basser PJ, Le Bihan D. Fiber orientation mapping in an anisotropic medium with NMR diffusion spectroscopy. In: Proc 11th Annual Meeting SMRM, Berlin, 1992. p 1221.
4. Jones DK, Williams SCR, Horsfield MA. Full representation of white matter fibre direction on one map via diffusion tensor analysis. In: Proc 5th Annual Meeting ISMRM, Vancouver, 1997. p 1743.
5. Pierpaoli C. Oh no! One more method for color mapping of fiber tract direction using diffusion MR imaging data. In: Proc 5th Annual Meeting ISMRM, Vancouver, 1997. p 1741.
6. Pajevic S, Pierpaoli C. Color schemes to represent the orientation of anisotropic tissues from diffusion tensor data: application to white matter fiber tract mapping in the human brain (published erratum appears in Magn Reson Med 2000;43:921). Magn Reson Med 1999;42: 526–540.
7. Mori S, Crain BJ, Chacko VP, van Zijl PC. Three dimensional tracking of axonal projections in the brain by magnetic resonance imaging. Ann Neurol 1999;45:265–269.
8. Conturo TE, Lori NF, Cull TS, Akbudak E, Snyder AZ, Shimony JS, McKinstry RC, Burton M, Raichle ME. Tracking neuronal fiber pathways in the living human brain. Proc Natl Acad Sci USA 1999;96: 10422–10427.
9. Jones DK, Simmons A, Williams SCR, Horsfield MA. Non-invasive assessment of axonal fiber connectivity in the human brain via diffusion tensor MRI. Magn Reson Med 1999;42:37–41.
10. Poupon C, Clark CA, Frouin V, Regis J, Bloch I, Le Bihan D, Mangin J. Regularization of diffusion-based direction maps for the tracking of brain white matter fasciculi. NeuroImage 2000;12:184–195.
11. Koch M, Glauche V, Finsterbusch J, Nolte U, Frahm J, Büchel C. Estimation of anatomical connectivity from diffusion tensor data. NeuroImage 2001;13:S176.

12. Tuch DS, Wiegell MR, Reese TG, Belliveau JW, Wedeen VJ. Measuring cortico-cortical connectivity matrices with diffusion spectrum imaging. In: Proc 9th Annual Meeting ISMRM, Glasgow, 2001. p 502.
13. Parker GJM, Barker GJ, Buckley DL. A probabilistic index of connectivity (PICo) determined using a Monte Carlo approach to streamlines. ISMRM Workshop Diffusion MRI: Biophysical Issues. St Malo, France, March, 2002.
14. Coulon O, Alexander D, Arridge SR. Principal diffusion direction field regularisation for diffusion tensor magnetic resonance images. In: Proc 9th Annual Meeting ISMRM, Glasgow, 2001. p 125.
15. Jones DK. A least squares continuous diffusion tensor field approximation. NeuroImage 2001;13:S168.
16. Pajevic S, Aldroubi A, Basser PJ. A continuous tensor field approximation of discrete DT-MRI data for extracting microstructural and architectural features of tissue. J Magn Reson 2002;154:85–100.
17. Wittenbrink CM, Pang AT, Lodha SK. Glyphs for visualizing uncertainty in vector fields. IEEE Trans Visual Comput Graph 1996;2:266–279.
18. Basser, PJ. Quantifying errors in fibre-tract direction and diffusion tensor field maps resulting from MR noise. In: Proc 5th Annual Meeting ISMRM, Vancouver, 1997. p 1740.
19. Efron B. Bootstrap methods: another look at the jackknife. Ann Statist 1979;7:1–16.
20. Pajevic S, Basser PJ. Non-parametric statistical analysis of diffusion tensor MRI data using the bootstrap method. In: Proc 7th Annual Meeting ISMRM, Philadelphia, 1999. p 1790.
21. Hasan KM, Parker DL, Alexander AL. Bootstrap analysis of DT-MRI encoding techniques. In: Proc 8th Annual Meeting ISMRM, Denver, 2000. p 789.
22. Lazar M, Hasan KM, Alexander AL. Bootstrap analysis of DT-MRI tractography techniques: streamlines and tensorlines. In: Proc 9th Annual Meeting ISMRM, Glasgow, 2001. p 1527.
23. Jones DK, Williams SCR, Gasston D, Horsfield MA, Simmons A, Howard R. Isotropic resolution diffusion tensor imaging with whole brain acquisition in a clinically acceptable time. Hum Brain Map 2002; 15:216–230.
24. Basser PJ, Matiello J, Le Bihan D. Estimation of the effective self-diffusion tensor from the NMR spin echo. J Magn Reson Ser B 1994; 103:247–254.
25. Basser PJ, Pajevic S. Statistical artefacts in diffusion tensor MRI (DT-MRI) caused by background noise. Magn Reson Med 2000;44:41–50.
26. Efron B. The jackknife, the bootstrap and other resampling methods, vol. 38. CBMS-NSF regional conference series in applied mathematics, SIAM, 1982.
27. Westin CF, Peled S, Gudbjartsson H, Kikinis R, Jolesz FA. Geometrical diffusion measures for MRI from tensor basis analysis. In: Proc 5th Annual Meeting ISMRM, Vancouver, 1997. p 1742.
28. Pierpaoli C, Basser PJ. Toward a quantitative assessment of diffusion anisotropy. Magn Reson Med 1996;36:893–906.
29. Basser PJ, Pierpaoli C. Microstructural and physiological features of tissue elucidated by quantitative-diffusion-tensor MRI. J Magn Reson B 1996;111:209–219.
30. Xu D, Mori S, Shen D, Davatzikos C. Statistically-based reorientation of diffusion tensor field. In: Proc IEEE International Symposium on Biomedical Imaging: Macro to Nano, Washington, DC, 2002. p 757–760.
31. Tuch DS, Weisskoff RM, Belliveau JW, Wedeen VJ. High angular resolution diffusion imaging of the human brain. In: Proc 7th Annual Meeting ISMRM, Philadelphia, 1999. p 321.
32. Wedeen VJ, Reese TG, Tuch DS, Weigell M, Dou J-G, Weisskoff RM, Chesler D. 2000. Mapping fiber orientation spectra in cerebral white matter with Fourier transform diffusion MRI. In: Proc 8th Annual Meeting ISMRM, Denver, 2000. p 82.